Enhanced mechanical properties of an Mg-Zn-Ca alloy via high pressure torsion and annealing for use in bone implantation

Congzheng Zhang[1] , Chen Liang[1] , Ting Liang [1] , Xinyu Si[1] , Chunqiang Jiang[1]

[1]Nanyang Normal University, School of Mechanical and Electrical Engineering, Wolong Street, n.1638, 473061, Nanyang, Henan, P.R.China.

e-mail: zcz1010@126.com, 76924997@qq.com, 2637196831@qq.com, 2829064470@qq.com, 2873616945@qq.com

ABSTRACT

The use of degradable magnesium alloy as a bone implant material has gained much research attention. However, its mechanical properties cannot meet the clinical requirements of bone implantation. In the present work, the microhardness, strength and plasticity of biological Mg-Zn-Ca alloy are evaluated before and after high pressure torsion (HPT) processing. The results demonstrate an obvious increase in the microhardness of the HPT-processed Mg-Zn-Ca alloy, with higher values distributed along the edge of the sample and low values in the center. After annealing, however, the microhardness value of the HPT Mg-Zn-Ca alloy decreases, but the distribution of microhardness values becomes significantly more uniform. The tensile test results show that the HPT processing increases the tensile strength of the Mg-Zn-Ca alloy, but decreases the toughness. When the HPT Mg-Zn-Ca alloy is annealed, however, the tensile strength decreases, while the plasticity noticeably increases, with increased annealing tempera-ture. The improvements in the strength and microhardness of the HPT Mg-Zn-Ca alloy are attributed to a combination of dislocation strengthening, fine grain strengthening, and precipitation strengthening. In conclusion, the Mg-Zn-Ca alloy has excellent comprehensive mechanical properties after 5 turns of HPT processing, followed by annealing at 210 °C for 30 min.

Keywords: Mg-Zn-Ca; Mechanical properties; High pressure torsion; Annealing.

1. INTRODUCTION

Recent interest has focused on degradable bone implantation materials for their ability to be absorbed in the human body, thus alleviating patient suffering, eliminating the need for a second operation, and reducing health-care costs [1–3]. The mechanical properties of the implant are gradually weakened due to degradation [4, 5]. Consequently, the supported load becomes transferred from the implant to the human bone and soft tissue, thus decreasing the stress-shielding effect [6–8]. At present, synthetic degradable polymers with a number of design improvements are widely used [9]. Nevertheless, the mechanical strength of the synthetic polymer remains lower than that of metal materials. Moreover, the polymeric implant cannot be detected by X-rays, so its deg-radation behavior in the human body is not observed [10]. In addition, individual differences among patients may result in non-specific foreign body reactions. Therefore, it is necessary to develop a novel degradable implantation material with good mechanical properties and biological safety, good binding and stability in the early stages of implantation, gradual degradation onset at the appropriate time, gradual reduction in mechanical properties, and eventual complete degradation within a predetermined time period.

The use of degradable magnesium alloy as a medical material has achieved rapid development, and this material is expected to eventually replace traditional metals and synthetic polymers. In particular, it is consid-ered to have the most revolutionary potential as a metal material for medical implants [11]. Degradable mag-nesium alloy has many advantages, including excellent biological behavior. Magnesium is a necessary element for the human body, and it is very concentrated in bones and teeth [12, 13]. Magnesium can strongly combine with phosphate to affect the mineralization of bone tissue by controlling the formation of hydroxyapatite [14]. In addition, the elastic modulus of magnesium is similar to that of human bone and provides a better match than titanium alloy, stainless steel, or Co-based alloys and, hence, greatly alleviates the stress shielding effect. More-over, Mg-based alloy is non-magnetic and will not interfere with techniques such as computed tomography or nuclear magnetic resonance [15, 16].

Nevertheless, the clinical application of magnesium alloy in bone implantation is limited by its fast degradation rate and poor mechanical properties [17]. To address these problems, global research has examined numerous approaches, such as alloying, surface treatment, and plastic deformation. However, although the new biomedical magnesium alloys have much better mechanical properties than pure magnesium, they are still unable to meet the requirements for clinical bone implantation [18, 19]. Furthermore, the addition of alloying elements may lead to the formation of second phases that undergo galvanic interactions with the matrix that tend to result in non-uniform degradation [20]. Although the degradation rate of magnesium alloy can be significantly decreased, and its biocompatibility enhanced, by surface treatment, this has no significant effect on the mechanical properties of the matrix [17, 21]. After plastic deformation, grain refinement can improve the mechanical properties of the metal material [22]. The grain size of magnesium alloy treated by traditional processing methods is usually about 10 μm due to its close-packed hexagonal structure. These traditional methods have limited effect on the fine grain strengthening of magnesium alloys. Hence, although the mechanical properties are improved, the requirements for clinical application in bone implantation remain unsatisfied. However, treatment by severe plastic deformation (SPD) induces more strain than traditional plastic deformation and can overcome the shortcomings of the traditional methods to refine the magnesium alloy into submicron even nanometer grains [23–25].

High pressure torsion (HPT) is a suitable treatment for materials that are difficult to deform [26, 27]. The metal sample is placed in a mold and subjected to a high pressure applied by a hydraulic mechanism, thus resulting in significant plastic deformation [28, 29]. This treatment enables materials with poor plasticity at room temperature (RT) to undergo a large amount of shear strain without fracturing [30, 31]. The induced shear strain remains in the material after HPT treatment, so that many materials that are intrinsically fragile at RT cannot be fractured after the treatment. As a result, the HPT process is very suitable for the magnesium alloys with very low deformability [32]. Consequently, HPT-treated magnesium alloys have recently attracted significant research interest [33]. Previous studies on the use of HPT-processed Mg-Zn-Ca alloy in bone implantation have demonstrated that the alloy trends to degrade uniformly in simulated body fluid (SBF), and that the degradation rate decreases over time. Moreover, the degradation process is distinct from the pitting corrosion of the as-cast magnesium alloy because the grain refinement and optimal distribution of the second phases during HPT lead to degradation of the entire surface of the alloy at a uniform and low rate. This promotes the formation of a compact, homogeneous layer of degradation products that protects the matrix from further degradation [34, 35]. In addition, the surface stress of the HPT-processed Mg-Zn-Ca alloy can be further decreased by post-HPT annealing. Hence, the tendency for stress corrosion cracking is further weakened, and the degradation rate is further decreased. In particular, these previous studies have demonstrated that the degradation rate of the HPT Mg-Zn-Ca alloy is the lowest when the annealing temperature is 210 °C [36].

In the present paper, the microstructures and mechanical properties of HPT Mg-Zn-Ca alloy are studied in order to elucidate the strengthening and toughening mechanisms of the HPT process. This work is seen as one useful contribution to the clinical application of magnesium alloy in bone implantation.

2. MATERIALS AND METHODS

The Mg-2Zn-0.22Ca (wt.%) alloy was selected for study because the Zn and Ca components are nontoxic to the human body. Zinc (Zn) is commonly incorporated into magnesium alloys to improve the alloy strength [37, 38]. In addition, Zn can weaken the effect of impurity elements on the alloy. Meanwhile calcium (Ca) is highly enriched in the human body and is mostly stored in the bones and teeth [39, 40]. Furthermore, Ca can promote the formation of new bone and increase the bone growth rate.

The Mg-Zn-Ca alloy ingot was prepared by semi-continuous casting. The solid solution state was obtained by subjecting the ingot to heating at a temperature of 420 °C for 60 h. Sample disks with 10-mm diameters and 0.82 mm thicknesses were prepared by mechanical turning, wire cutting, and polishing. These samples were then subjected to 1, 2, and 5 turns of HPT processing under 7.5 GPa at 0.5 rpm. Finally, the HPT alloys were annealed at various temperatures (90–270 °C) for 30 min, followed by air-cooled to ambient temperature.

The microstructures were studied via optical microscopy (OM), scanning electron microscopy (SEM), and transmission electron microscopy (TEM). For the SEM (Quanta2000), the samples were polished to ~50 μm by abrasive paper and etched by 4% Nital (nitric acid + alcohol). For the TEM (JEM2100), the samples were punched into numerous 3-mm diameter disks, which were then subjected to ion thinning.

The microhardness was tested using a Vickers microhardness meter under an applied stress of 0.981N for 15 s. As shown in Figure 1, the microhardness was tested along the diameter at sites spaced 0.3 mm apart (white circles) starting from the center and moving towards the two edges, for a total of 33 measurement points. For
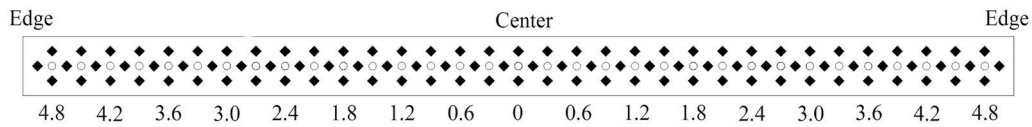
Edge   Center   Edge

4.8   4.2   3.6   3.0   2.4   1.8   1.2   0.6   0   0.6   1.2   1.8   2.4   3.0   3.6   4.2   4.8

Figure 1: The schematic diagram of microhardness measured points.
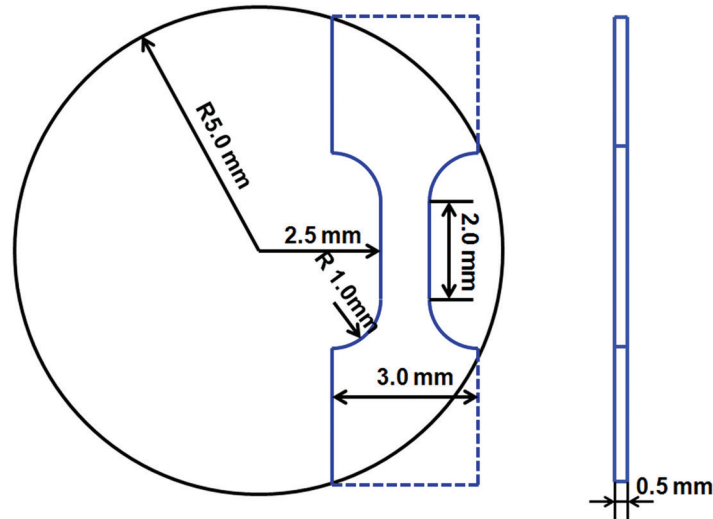
R5.0 mm

2.5 mm

R 1.0mm

2.0 mm

3.0 mm

0.5 mm

Figure 2: The specification of tensile sample of Mg-Zn-Ca alloy.

Figure 3: The clamping mould in tensile test.

each site, tests were performed at four positions with a spacing of 0.15 mm (black dots). The average microhardness value of the four black points was then considered to be the Vickers microhardness value of the white site.

The mechanical properties were tested using a tensile testing machine. As shown in Figure 2, the dimensions of the Mg-Zn-Ca alloy test samples were $0.5 \times 1 \times 2$ mm (thickness × width × length). As this is relatively small, the requirements of the relevant ISO standard were not satisfied. Hence, the obtained tensile test results for the HPT Mg-Zn-Ca alloy can only be qualitatively compared with those of the same sized samples, and cannot be quantitatively compared with those of the international standard samples. Prior to the test, the tensile samples were processed by wire cutting at a rate of 150 steps/s. Due to the small size, each tensile sample had to be placed in special mold, as shown in Figure 3. This was then clamped to the tensile testing machine, and the samples was tested at a tensile rate of 0.2 mm/min.

3. RESULTS AND DISCUSSION

3.1. Microstructure

The microstructural morphology of the Mg-Zn-Ca alloy in the solid solution state is revealed by the OM images in Figure 4. Here, the grains are seen to be equiaxed with a calculated average grain size of 85 μm. The grain growth
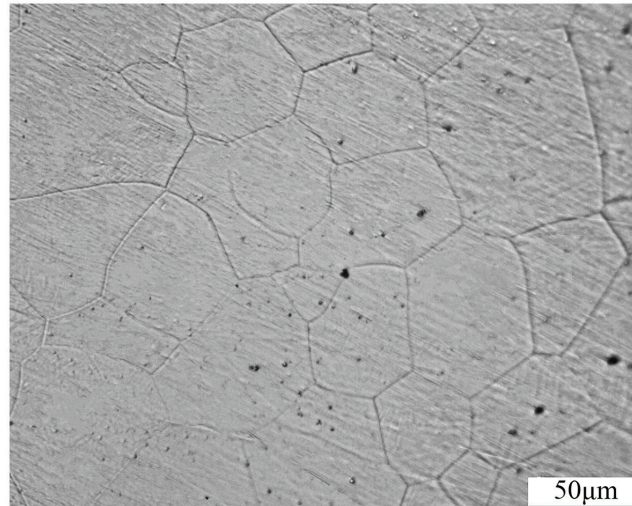
Figure 4: The microstructure of Mg-Zn-Ca alloy before high pressure torsion.
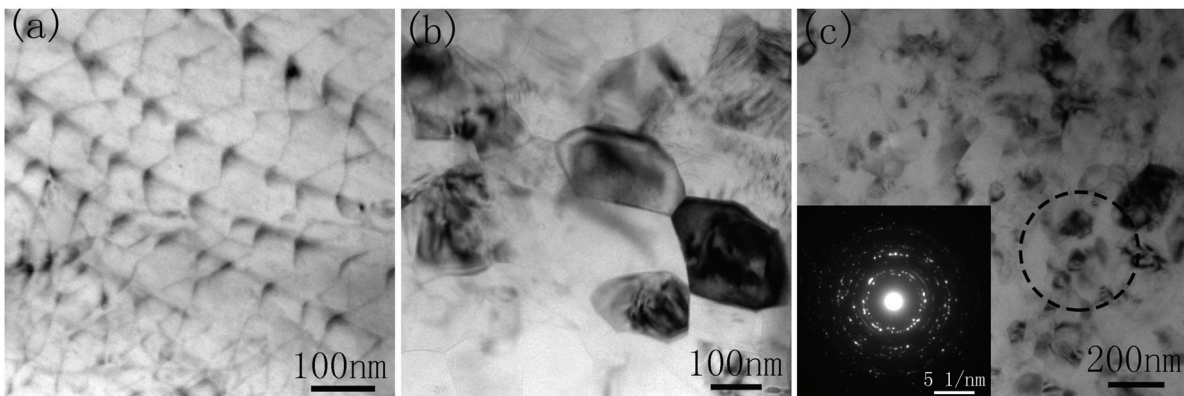

Figure 5: The microstructure of Mg-Zn-Ca alloy after high pressure torsion.

during solution treatment is not significant, and no stripy second phases are observed along the grain boundaries (GBs). This is because the second phases are mostly dissolved into the Mg matrix during the heat treatment.

By contrast, the TEM images in Figure 5(a) reveal the appearance of numerous tangled dislocation lines due to the large shear strain accumulated during 1 turn of HPT processing. Thus, the HPT process leads to the formation of a dislocation entanglement zone. Although the dislocation lines are initially chaotic and irregular. The dislocations begin to interact with each other as their number increases. Hence, after dislocation annihilation and recombination, the dislocation arrangement becomes somewhat orderly, and the dislocations are ready to transform into dislocation cells or to align along the GBs. Thus, as shown in Figure 5(b), the dislocation cells and sub-GBs have transformed into GBs after 2 turns of HPT, and some fine grains are seen to have already formed. Further, when the total number of HPT turns is increased to 5, the cumulative shear strain becomes very large, and the misorientations of the sub-GBs gradually increase via continuous absorption of the dislocations, thus gradually forming large-angle GBs. This, in turn, leads to the formation of numerous fine grains, as shown in Figure 5(c). In addition, the SAED pattern (inset, Figure 5(c)) exhibits a clear diffraction ring indicative of complete grain refinement to form a polycrystalline alloy. Measurement using a Nano-Measurer followed by statistical analysis and calculation indicates a fine grain size of between 70 and 110 nm, with an average grain size of 94 nm.

The morphologies of the 5-turn HPT-processed Mg-Zn-Ca alloy after annealing at various temperatures are revealed by the TEM images in Figure 6(b−h). Here, the annealed Mg-Zn-Ca alloy continues to exhibit equi-axed grains, and these are seen to increase in size as the annealing temperature is increased (Figure 6(i)). Before annealing, the average grain size of the HPT alloy is 94 nm (Figure 6(a)). Moreover, the grain sizes of the alloy after annealing at 90 °C and 120 °C are 136 nm and 161 nm, respectively. Grain growth is not significant at a low annealing temperature (Figure 6(b–c)). With the further increase of annealing temperature, the average grain
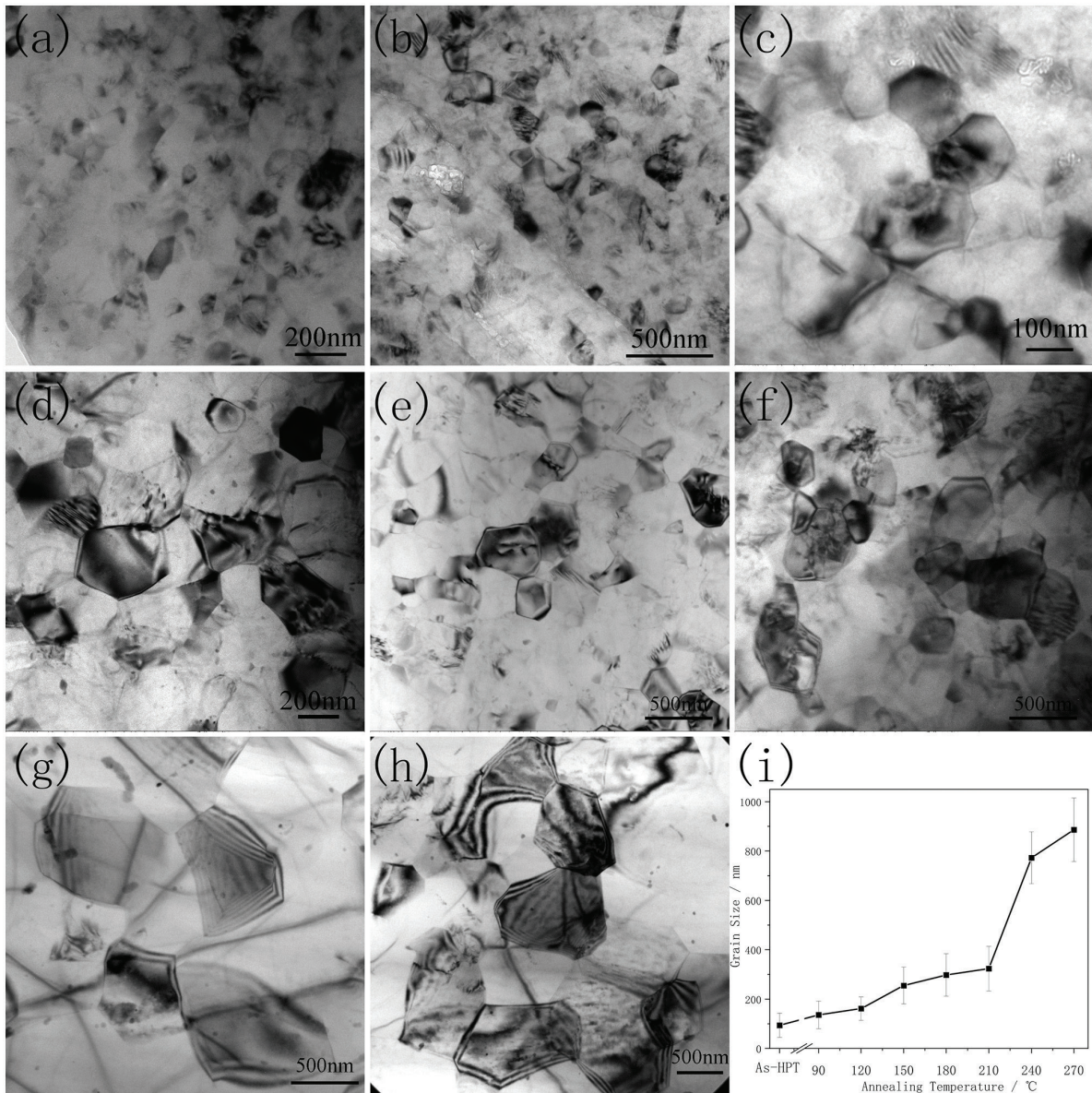
Figure 6: TEM morphology of HPT alloy before and after annealing: (a) as-HPT, (b) 90 °C, (c) 120 °C, (d) 150 °C, (e) 180 °C, (f) 210 °C, (g) 240 °C, (h) 270 °C; (i) Grain Size of HPT alloy before and after annealing.

sizes continue to increase to 254 nm, 298 nm and 323 nm respectively at 150 °C, 180 °C and 210 °C annealing temperatures. However, grain growth becomes extremely significant at an annealing temperature above 210 °C. The grain sizes increase remarkably to 773 nm and 886 nm at annealing temperatures of 240 °C and 270 °C. Similar results have been previously reported by H. Iwaoka for the post-HPT annealing of palladium, where minimal grain growth was observed at temperatures under 200 °C, but rapid grain growth was observed at temperatures above 200 °C [41]. Thus, both the present experimental results and the previously-published reports demonstrate the existence of a critical annealing temperature for HPT-processed alloys. When the annealing is performed below this critical temperature, there is little increase in the grain size of the HPT alloy; above this critical temperature, however, obvious and significant grain growth is achieved.

The morphologies of the 5-turn HPT-processed Mg-Zn-Ca alloy after various annealing temperatures are further revealed by the TEM images in Figure 6(a−h). Here, the uniform distribution of the second phase particles can be clearly observed. Moreover, the number of second phase particles is seen to initially increase, and subsequently decrease, with increasing annealing temperature. Thus, while little change is observed at low annealing temperatures (90−120 °C), a clear increase is seen at moderate temperatures(150−210 °C). For the Mg-Zn-Ca alloy in the solid solution state, the annealing treatment in the latter temperature range also plays the role of artificial aging, which leads to significant precipitation of the second phase from the solid solution.
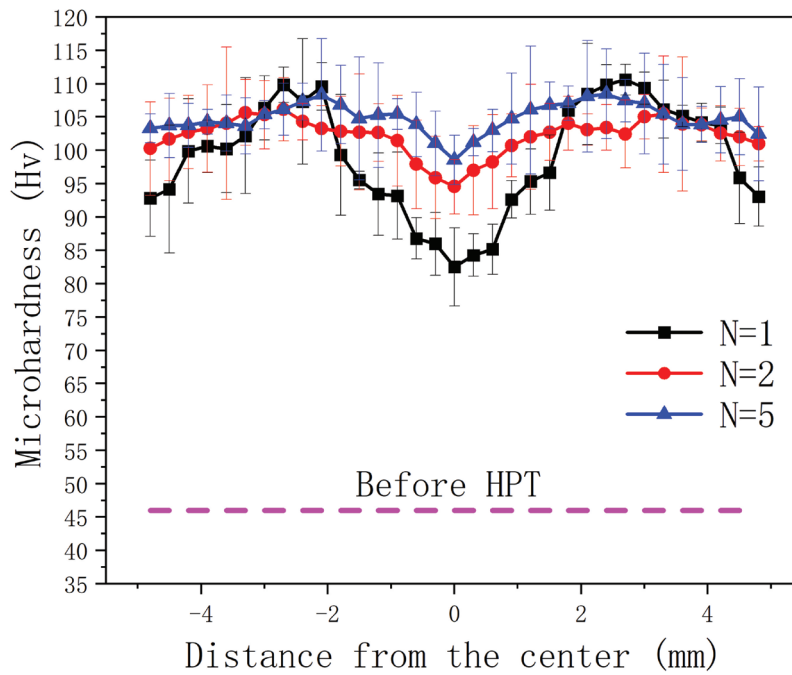
Figure 7: The microhardness distribution of Mg-Zn-Ca alloy before and after HPT.

Therefore, the second phases are provided by both the stress-induced precipitation during the HPT processing and the artificial aging precipitation during the annealing treatment. However, as the temperature rises further (240−270 °C), the quantity of second phase particles begins to decrease, such that few remain when the annealing temperature reaches 270 °C. This is because the precipitated second phase particles are small and easy to dissolve back into the matrix under a sufficiently high annealing temperature.

3.2. Microhardness

The microhardness distributions of the Mg-Zn-Ca alloy along the diameter before and after one, two, and five turns of HPT processing are indicated in Figure 7. Although the microhardness is seen to have doubled after one turn of HPT (N = 1), there is a clear distribution of low values at the center of the sample and high values along the edges. The increase in microhardness with HPT treatment can be attributed to the aggregation of a large number of dislocations near the GBs, where they become entangled with each other to form a chaotic dislocation zone, as seen in Figure 5. This high dislocation density will directly increase the hardness value. However, the shear stresses will vary significantly across the HPT alloy, being low in the center and large at the edge, thus explaining the observed microhardness distribution. Further, the microhardness value is seen to decrease towards the outermost region because there is a gap between the upper and lower anvils, which results in edge fins on the periphery of the disks.

After two turns of HPT (N = 2), the microhardness is further increased, but continues to show a distribution of low values at the center of the sample and high values at the edges. Nevertheless, some fine grains are present and complete refinement has occurred in some isolated regions. Because the shear stress is much higher at the edges than that in the center, the refinement process begins at the edge and gradually proceeds towards the center. The homogeneity of the alloy is improved as the refinement becomes complete. According to the changes in the microhardness values, the surface of the alloy can be sub-divided into a hardening region (where the microhardness value is gradually increasing from the center to the edge) and a steady-state region (where a maximum microhardness has been achieved and is maintained). Compared to the situation after 1 turn of HPT, 2 turns of HPT result in shrinkage of the hardening region and the microhardness value reaches the steady state at about 2 mm from the center. Even after five turns of HPT (N = 5), the microhardness distribution along the diameter remains high at the edge and low in the center. However, the homogeneity is significantly improved compared to that obtained after 1 and 2 turns of HPT. Moreover, although the microhardness is not changed very much at the edge, that at the center is seen to be significantly improved. In addition, the hardening region has become smaller, such that the microhardness becomes stable at 1 mm from the center, due to the near completion of the grain refinement process. There are a few differences in morphologies between the center and the edge.
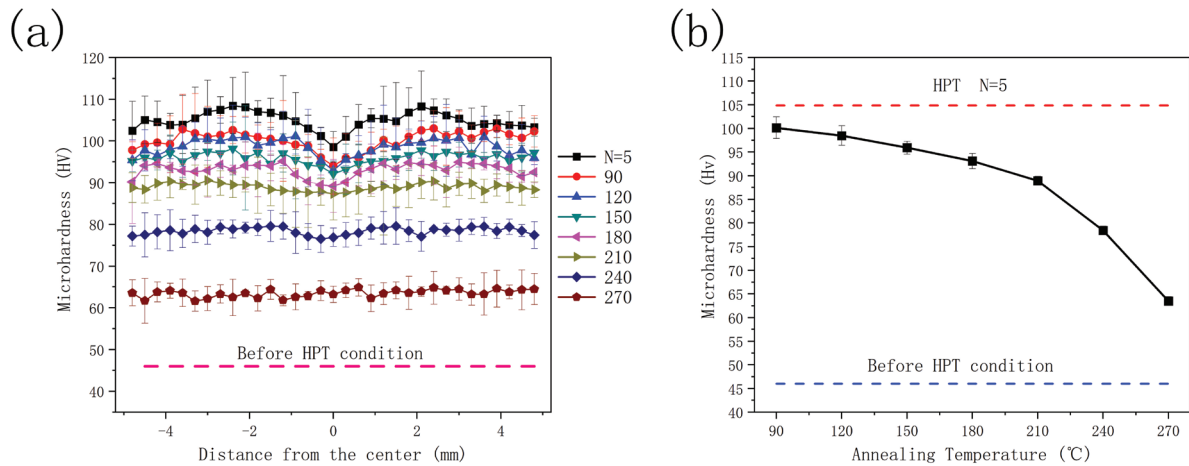
(a)

(b)

Figure 8: (a) The microhardness distribution of Mg-Zn-Ca alloy before and after HPT; (b) the average microhardness value of Mg-Zn-Ca alloy.

Thus, the microhardness of the Mg-Zn-Ca alloy varies with the dislocation density and is closely related to the processes of dislocation proliferation, aggregation, entanglement and annihilation. In the early stages of HPT process, dislocations start to proliferate, the dislocation density increases rapidly, and the process of work hardening plays a significant role. Therefore, the microhardness increases rapidly. As the number of HPT turns increases from 1 to 2, the dislocations begin to aggregate and tangle with each other, while both the dislocation density and the microhardness continue to increase. Finally, as the number of HPT turns increases to 5, the dislocations are transformed into GBs or dislocation cells. At this stage, the processes of dislocation proliferation and dislocation annihilation reach a dynamic balance and, hence, the dislocation density remains stable even under a continuously increasing shear strain .

The microhardness of the Mg-Zn-Ca alloy is also influenced by the second phases. Before the HPT, the Mg-Zn-Ca alloy is in the solid solution state, with all components being completely dissolved in the Mg matrix; hence, there are no second phases. During the HPT process, however, some relatively small and densely distributed second phase particles precipitate out from the solid solution under the action of shear strain, thus further increasing the microhardness via precipitation strengthening.

The effects of annealing upon the 5-turn HPT-processed Mg-Zn-Ca alloy are clearly revealed in Figure 8(a), where the microhardness distribution along the diameter is more uniform after annealing. Furthermore, the difference in microhardness between the center and the edge is seen to gradually diminish with increased annealing temperature. At the same time, the distribution of microhardness values becomes more uniform, but the absolute microhardness of the HPT alloy is slightly decreased. Thus, at low annealing temperatures (90−180℃), the microhardness of the HPT alloy remains high at the edge and low in the center. Moreover, the decrease in hardness with increased annealing temperature is slower in the central region and faster towards the edge, thus helping to increase the uniformity of the microhardness distribution. However, the large number of lattice defects at the edge of the alloy due to the high shear stress during HPT processing can be significantly reduced even at a low annealing temperature. The shear strain is theoretically very low in the center, so there are few defects there. As a result, the microhardness declines only slightly and the change is not obvious.

In brief, the significantly improved microhardness of the HPT-processed Mg-Zn-Ca alloy is attributed to the following three reasons: (i) the work hardening effect of the numerous defects generated by the processing, (ii) the significant strengthening provided by grain refinement, and (iii) precipitation strengthening due to the uniform distribution of the second phases. While the first of these effects can be eliminated by low temperature annealing, the second remains very strong because grain growth is very slow, as indicated by the microstructural analysis. This analysis also reveals that more second phases have precipitated from the Mg matrix after annealing at 90−210 ℃ due to artificial aging, thus potentially compensating for the decrease in microhardness. When the annealing temperature reaches 210 °C, however, the microhardness is seen to have decreased slightly in the central region and significantly in the edge region, compared to that at 180 °C. These effects result in similar microhardness values at the edge and the center, thus providing a significantly improved, uniform microhardness distribution. At annealing temperatures above 240 ℃, the uniformity of the HPT alloy remains very fine, but the microhardness begins to decrease significantly. The microstructural analysis indicates that the previously dispersed solid precipitation phases are dissolved back into the matrix with increasing annealing temperature.
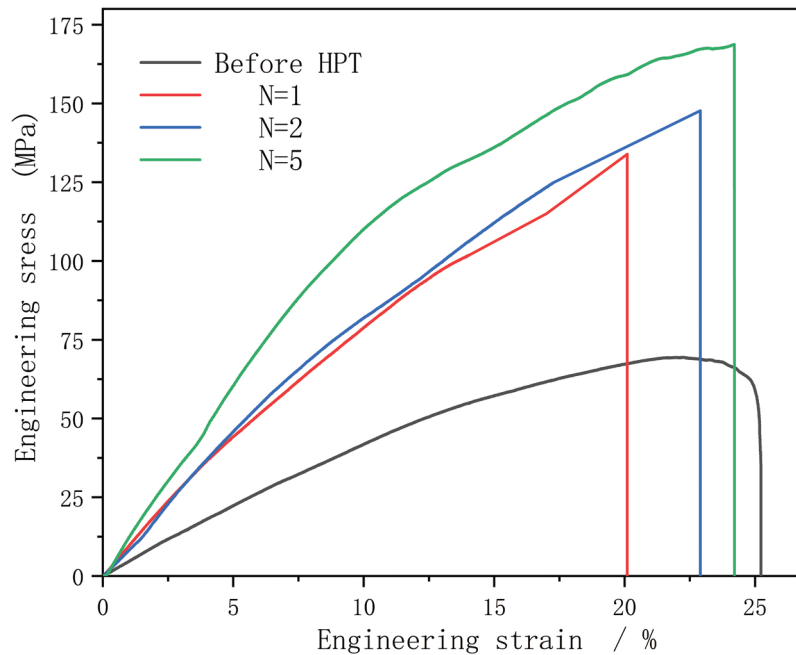
Figure 9: The stress-strain curves of Mg-Zn-Ca alloy before and after HPT.

This contributes a slight decrease in the microhardness due to the loss of the precipitation strengthening effect. In addition, the grain growth increases rapidly when the temperature is above 210 °C, thus significantly reducing the fine-grain strengthening effect and significantly decreasing the microhardness.

The calculated average microhardness values of Mg-Zn-Ca alloy are presented in Figure 8(b). Thus, when the annealing temperature is above 210 °C, the average microhardness rapidly decreases and eventually approaches that of the pre-HPT alloy. At this stage, work-hardening is eliminated, and the precipitation strengthening and fine-grain strengthening are significantly weakened. At annealing temperatures below 210 °C, however, these effects are compensated by an increase in the precipitation strengthening. These results demonstrate that the annealing temperature must not be allowed to exceed 210 °C, as otherwise the microhardness of the Mg-Zn-Ca HPT alloy will decrease too much. At annealing temperatures of 180−210 °C, a uniform microhardness distribution is achieved for the HPT alloy.

3.3. Strength and toughness

The results presented in Figure 9 reveal a significant improvement in the ultimate tensile strength (UTS) of the Mg-Zn-Ca alloy from 69.4 MPa before HPT to 168.8 MPa after 5 turns of HPT. This is attributed to the following three reasons: (i) the very notable work hardening effect of the HPT process at RT, (ii) the significant fine-grain strengthening due to grain refinement during the HPT processing, and (iii) the precipitation and uniform distribution of second phase particles along the grain boundaries, which can pin the GBs and, thus, provide precipitation strengthening. The precipitated second phases have a small size and a coherent relationship with the Mg matrix. According to the interaction mechanism between the dislocations and precipitated phases, it is inferred that the precipitated second phase particles are cut across by the moving dislocations. This increases the friction between the dislocation and the crystal lattice, thereby hindering the movement of the dislocation.

The results in Figure 9 further indicate that the UTS of the Mg-Zn-Ca HPT alloy increases with increasing number of HPT turns. After 1 turn, a large number of dislocations have gathered and become entangled with each other close to the GBs, thereby merging to generate a dislocation entanglement zone. As the dislocation density of the HPT-processed alloy is much higher than that of the pre-HPT alloy, the UTS is correspondingly improved. After 2 turns of HPT, the accumulation of shear strain further increases the dislocation density and, hence, the UTS. Finally, after 5 turns of HPT, dislocation proliferation and annihilation are in dynamic equilibrium and have resulted in the formation of sub-GBs and dislocation cells. Thus, the grain refinement of the Mg-Zn-Ca alloy is completed and the UTS is further enhanced.

The results presented in Figure 9 indicate a clear reduction in the plasticity of the Mg-Zn-Ca alloy after 1 turn of HPT at RT. This is attributed to the relatively large residual stress caused by the numerous lattice defects. In addition, an increase in the number of turns of HPT leads to further improvement in the plasticity improves due
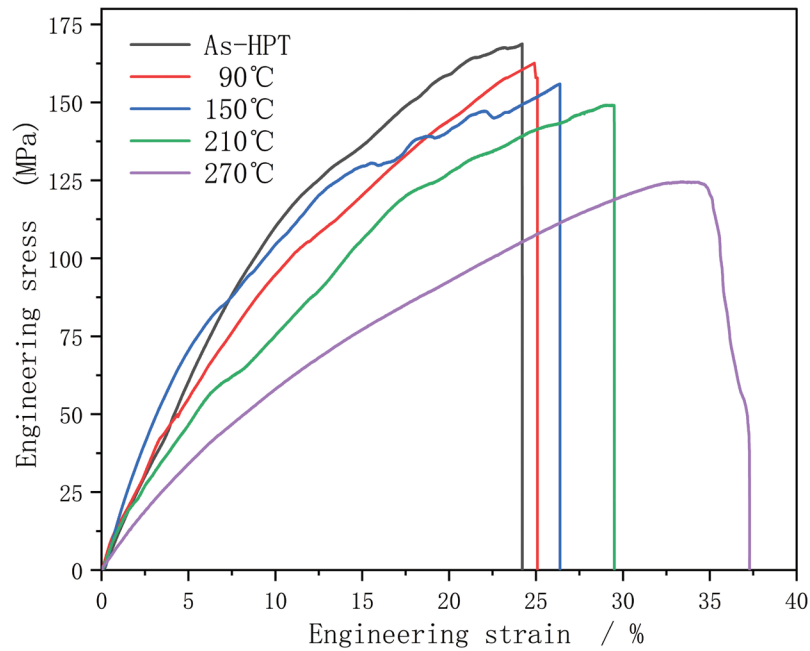
Figure 10: The stress-strain curves of Mg-Zn-Ca alloy processed by high pressure torsion before and after annealing.

to the beneficial grain refinement. Notably, the results presented in Figure 9 indicate that the elongation of the pre-HPT Mg-Zn-Ca alloy is close to 25.2%. It is worth pointing out that HPT alloy disks used in the present study were small, and the size of the tensile specimens was non-standard. This leads to a severe size effect during the tensile test, thus resulting in some experimental error, especially with respect to the plasticity value. Therefore, the results of the tensile test, and particularly the plasticity test, can only be qualitatively compared with those obtained for samples of the same size, and cannot be quantitatively compared with those obtained using the standard sample size. Moreover, the stress-strain curves presented in Figure 9 are not smooth and exhibit clear fluctuations. This is because the mold for positioning the tensile sample was small, and the clamping area between the chuck and the mold was also relatively small. Therefore, a slight slippage can easily occur between the chuck and the mold during the tensile test, thus reducing the smoothness of the obtained curve and introducing experimental error into the test results.

The stress-strain test results for the 5-turns HPT-processed Mg-Zn-Ca alloy after annealing at various temperatures are presented in Figure 10. Here, the UTS is seen to decrease gradually with increased annealing temperature. In detail, a slow decrease in UTS is observed at annealing temperatures below 210 °C, with a very fast decrease occurring at annealing temperatures above 210 °C. This can be explained in terms of the observed microstructural morphologies, where the grain size increases slowly at annealing temperatures below 210 °C, thus limiting the effect of fine-grain strengthening. As noted above, this effect is compensated to some extent by the gradual precipitation of more second phase particles. When the annealing temperature is above 210 °C, however, the grain size increases significantly, and the second phases gradually dissolve back into the Mg matrix. This limits both the fine grain strengthening and precipitation strengthening effects. Thus, although the solution strengthening is improved, it can only slightly compensate for the decline in UTS; hence, the UTS is significantly reduced.

Overall, the plasticity of the HPT-processed Mg-Zn-Ca alloy increases with increased annealing temperature because the annealing treatment eliminates the crystal defects. When the annealing temperature is 90 °C, the elongation of the HPT alloy is close to that of the solid-solution alloy before the HPT process. As the annealing temperature is increased to 150 °C, however, the elongation of the alloy exceeds that of solid-solution alloy. Finally, when the annealing temperature is 210 °C, the UTS of the HPT alloy is 149.8 MPa, which is 12.7% lower than that of the non-annealed HPT alloy but 115% higher than that of the pre-HPT solid-solution alloy. In addition, the elongation is 22.8% higher than that of the non-annealed HPT alloy and 17.5% higher than that of the pre-HPT solid-solution alloy. In conclusion, the strength and plasticity of the Mg-Zn-Ca alloy can be optimized by the application of turns of 5 HPT and subsequent annealing at 210 °C.

4. CONCLUSIONS

For clinical application in bone implantation, the Mg-Zn-Ca alloy biomaterials are required to have excellent mechanical properties. In this work, the biological Mg-Zn-Ca alloy was processed via high pressure torsion (HPT) at room temperature (RT) to generate an ultrafine-grained bulk alloy. After HPT processing, the

microhardness of the Mg-Zn-Ca alloy is found to be twice that of the pre-HPT alloy. However, the microhardness exhibits a non-uniform distribution, being low at the center and high at the edge of the HPT alloy. Nevertheless, the microhardness is shown to further increase, and the distribution become more uniform, with increasing number of turns of HPT. The largest average microhardness is obtained by the application of 5 turns of HPT.

The effects of post-HPT annealing at various temperatures were also investigated, and the microhardness of the alloy was shown to decrease with increased annealing temperature. However, the uniformity of the microhardness distribution was improved significantly. Thus, an annealing temperature of 210 °C was found to provide a good uniformity of microhardness with minimal decrease in the actual microhardness value.

In addition, the ultimate tensile strength (UTS) of the Mg-Zn-Ca alloy was shown to gradually increase with increasing number of turns of HPT, while the plasticity showed a trend of initial decrease and later increase. After 5 turns of HPT, the grain refinement was compete, thus enhancing the plasticity. In addition, the UTS was found to further decrease, and the plasticity increase, with increased annealing temperature. When the annealing temperature was 210 °C, the plasticity was significantly improved without much reduction in the UTS.

The improvement in strength and microhardness of the HPT-processed Mg-Zn-Ca alloy was attributed to the combined effects of dislocation strengthening, fine-grain strengthening, and precipitation strengthening. Many dislocations are formed during the HPT process at RT, and the interactions between these dislocations result in the formation of dislocation jogs. Some dislocation jogs and fixed dislocations act as strong obstacles to the movement of dislocations; hence, dislocation aggregation readily occurs and the work-hardening rate is high. Moreover, in polycrystalline materials, grain boundaries (GBs) have a good resistance to deformation and provide further resistance to dislocation movement, since it is difficult for dislocations to cut through the GBs. Hence, the increase in the total area of GBs after grain refinement leads to an increased strength of the alloy, and the stress-induced precipitation of second phase particles further helps to pin the GBs. These principles also explain the initial increase and subsequent decrease in plasticity with the increasing number of turns of HPT. In the initial stage of processing, the increase in dislocation density and the precipitation of second phase particles along the GBs suppress the plastic deformation ability, thus decreasing the plasticity. However, once the grain refinement is complete, the plasticity is improved. Based on the results of microhardness and tensile testing, the Mg-Zn-Ca alloy exhibited excellent mechanical properties after 5 turns of HPT followed by annealing at 210 °C for 30 min.

5. ACKNOWLEDGMENTS

6. BIBLIOGRAPHY

[1]   KIRKLAND, N.T., BIRBILIS, N., STAIGER, M.P., "Assessing the corrosion of biodegradable magnesium implants: a critical review of current methodologies and their limitations", *Acta Biomaterialia*, v. 8, n. 3, pp. 925–936, 2012.

[2]   SEDELNIKOVA, M.B., UGODCHIKOVA, A.V., TOLKACHEVA, T.V.*, et al.*, "Surface modification of Mg0.8Ca alloy via wollastonite micro-arc coatings: significant improvement in corrosion resistance", *Metals*, v. 11, n. 5, 754, 2021.

[3]   FARÈ, S., GE, Q., VEDANI, M.*, et al.*, "Evaluation of material properties and design requirements for biodegradable magnesium stents", *Matéria (Rio J.)*, v. 15, pp. 96–103, 2010.

[4]   HO, Y., JOSHI, S.S., WU, T.*, et al.*, "In-vitro bio-corrosion behavior of friction stir additively manufactured AZ31B magnesium alloy-hydroxyapatite composites", *Materials Science and Engineering: C*, v. 109, pp. 110632, 2020.

[5]   BOMMALA, V.K., KRISHNA, M.G., RAO, C.T., "Magnesium matrix composites for biomedical applications: A review", *Journal of Magnesium and Alloys*, v. 7, n. 1, pp. 72–79, 2019.

[6]   ALI, M., HUSSEIN, M.A., AL-AQEELI, N., "Magnesium-based composites and alloys for medical applications: A review of mechanical and corrosion properties", *Journal of Alloys and Compounds*, v. 792, pp. 1162–1190, 2019.

[7]   KATARIVAS LEVY, G., GOLDMAN, J., AGHION, E., "The prospects of zinc as a structural material for biodegradable implants – a review paper", *Metals*, v. 7, n. 10, 402, 2017.

[8]   BEILNER, G., PEREIRA, B.L., LEPIENSKI, C.M.*, et al.*, "Ti-25Nb-25Ta alloy treated by plasma electrolytic oxidation in phosphoric acid for implant applications", *Matéria (Rio J.)*, v. 26, n. 1, e12933, 2021.

[9] GUNATILLAKE, P., MAYADUNNE, R., ADHIKARI, R., "Recent developments in biodegradable synthetic polymers", *Biotechnology annual review*, v. 12, pp. 301–347, 2006.

[10] ENGELBERG, I., KOHN, J., "Physico-mechanical properties of degradable polymers used in medical applications: A comparative study", *Biomaterials*, v. 12, n. 3, pp. 292–304, 1991.

[11] CHAKRABORTY BANERJEE, P., AL-SAADI, S., CHOUDHARY, L., *et al.*, "Magnesium implants: prospects and challenges", *Materials*, v. 12, n. 1, 136, 2019.

[12] LI, L., CUI, L., ZENG, R., *et al.*, "Advances in functionalized polymer coatings on biodegradable magnesium alloys – A review", *Acta Biomaterialia*, v. 79, pp. 23–36, 2018.

[13] JAMEL, M.M., JAMEL, M.M., LOPEZ, H.F., "Designing advanced biomedical biodegradable Mg alloys: a review", *Metals*, v. 12, n. 1, 85, 2022.

[14] YADAV, V. S., KUMAR, A., DAS, A., *et al.*, "Degradation kinetics and surface properties of bioceramic hydroxyapatite coated AZ31 magnesium alloys for biomedical applications", *Materials Letters*, v. 270, 127732, 2020.

[15] LEIGHEB, M., VENEZIANO, M., TORTIA, R., *et al.*, "Osteosynthesis devices in absorbable magnesium alloy in comparison to standard ones: a systematic review on effectiveness and safety", *Acta Bio-Medica : Atenei Parmensis*, v. 92, suppl 3, e2021025, 2021.

[16] PANEMANGALORE, D.B., SHABADI, R., GUPTA, M., "Corrosion behavior, microstructure and mechanical properties of novel Mg-Zn-Ca-Er alloy for bio-medical applications", *Metals*, v. 11, n. 3, 519, 2021.

[17] WAN, P., TAN, L., YANG, K., "Surface modification on biodegradable magnesium alloys as orthopedic implant materials to improve the bio-adaptability: a review", *Journal of Materials Science & Technology*, v. 32, n. 9, pp. 827–834, 2016.

[18] BAKHSHESHI-RAD, H.R., IDRIS, M.H., ABDUL-KADIR, M.R., *et al.*, "Mechanical and bio-corrosion properties of quaternary Mg–Ca–Mn–Zn alloys compared with binary Mg–Ca alloys", *Materials & Design*, v. 53, pp. 283–292, 2014.

[19] JANBOZORGI, M., TAHERI, K.K., TAHERI, A.K., "Microstructural evolution, mechanical properties, and corrosion resistance of a heat-treated Mg alloy for the bio-medical application", *Journal of Magnesium and Alloys*, v. 7, n. 1, pp. 80–89, 2019.

[20] DING, Y., LI, Y., WEN, C., "Effects of Mg17Sr2 phase on the bio-corrosion behavior of Mg–Zr–Sr alloys", *Advanced Engineering Materials*, v. 18, n .2, pp. 259–268, 2016.

[21] TANG, Y., ZHU, L., ZHANG, P., *et al.*, "Enhanced corrosion resistance of bio-piezoelectric composite coatings on medical magnesium alloys", *Corrosion Science*, v. 176, pp. 108939, 2020.

[22] WU, P., XU, F., DENG, K., *et al.*, "Effect of extrusion on corrosion properties of Mg-2Ca-χAl (χ= 0, 2, 3, 5) alloys", *Corrosion Science*, v. 127, pp. 280–290, 2017.

[23] JOZEF, Z., SERGEY, D.V., GEORGE, R., *et al.*, "Ultrafine grained structure development in steel with different initial structure by severe plastic deformation", *Matéria (Rio J.)*, v. 15, pp. 240–246, 2010.

[24] TORABI, H., HOSEINI, M., SADRKHAH, M., *et al.*, "Microstructure, mechanical properties and bio-corrosion properties of Mg-HA bionanocomposites fabricated by a novel severe plastic deformation process", *Ceramics International*, v. 46, n. 3, pp. 2836–2844, 2020.

[25] KAVYANI, M., EBRAHIMI, G.R., EZATPOUR, H.R., *et al.*, "Microstructure refinement, mechanical and biocorrosion properties of Mg–Zn–Ca–Mn alloy improved by a new severe plastic deformation process", *Journal of Magnesium and Alloys*, in press, 2021.

[26] GORNAKOVA, A.S., STRAUMAL, B.B., MAZILKIN, A.A., *et al.*, "Phase composition, nanohardness and young's modulus in Ti-Fe alloys after heat treatment and high pressure torsion", *Metals*, v. 11, n. 10, pp. 1657, 2021.

[27] FIGUEIREDO, R.B., LANGDON, T.G., "Processing magnesium and its alloys by high-pressure torsion: an overview", *Advanced Engineering Materials*, v. 21, n. 1, 1801039, 2019.

[28] LIU, Y., LIU, M., CHEN, X., *et al.*, "Effect of Mg on microstructure and mechanical properties of Al-Mg alloys produced by high pressure torsion", *Scripta Materialia*, v. 159, pp. 137–141, 2019.

[29] CARVALHO, A.P., REIS, L.M., PINHEIRO, R.P.R.P., *et al.*, "Using plane strain compression test to evaluate the mechanical behavior of magnesium processed by HPT", *Metals*, v. 12, n. 1, pp. 125, 2022.

[30] MOHAMED, I.F., MASUDA, T., LEE, S., *et al.*, "Strengthening of A2024 alloy by high-pressure torsion and subsequent aging", *Materials Science and Engineering: A*, v. 704, pp. 112–118, 2017.

[31] SILVA, C.L.P., CAMARA, M.A., HOHENWARTER, A.*, et al.*, "Mechanical behavior and in vitro corrosion of cubic scaffolds of pure magnesium processed by severe plastic deformation", *Metals*, v. 11, n. 11, 1791, 2021.

[32] OJDANIC, A., HORKY, J., MINGLER, B.*, et al.*, "The effects of severe plastic deformation and/or thermal treatment on the mechanical properties of biodegradable Mg-alloys", *Metals*, v. 10, n. 8, 1064, 2020.

[33] LUKYANOVA, E.A., MARTYNENKO, N.S., SHAKHOVA, I.*, et al.*, "Strengthening of age-hardenable WE43 magnesium alloy processed by high pressure torsion", *Materials Letters*, v. 170, pp. 5–9, 2016.

[34] ZHANG, C.Z., ZHU, S.J., WANG, L.G.*, et al.*, "Microstructures and degradation mechanism in simulated body fluid of biomedical Mg–Zn–Ca alloy processed by high pressure torsion", *Materials & Design*, v .96, pp. 54–62, 2016.

[35] ZHANG, C., GUAN, S., WANG, L.*, et al.*, "Effect of solution pretreatment on homogeneity and corrosion resistance of biomedical Mg-Zn-Ca alloy processed by high pressure torsion", *Advanced Engineering Materials*, v. 19, n. 1, 1600326, 2017.

[36] ZHANG, C., GUAN, S., WANG, L.*, et al.*, "The microstructure and corrosion resistance of biological Mg–Zn–Ca alloy processed by high-pressure torsion and subsequently annealing", *Journal of Materials Research*, v. 32, n. 6, pp. 1061–1072, 2017.

[37] SPIGARELLI, S., REGEV, M., EVANGELISTA, E.*, et al.*, "Review of creep behaviour of AZ91 magnesium alloy produced by different technologies", *Materials Science & Technology*, v. 17, n. 6, pp. 627–638, 2001.

[38] SONG, G.L., ATRENS, A., "Corrosion mechanisms of magnesium alloys", *Advanced Engineering Materials*, v. 1, n. 1, pp. 11–33, 1999.

[39] DRYNDA, A., HASSEL, T., HOEHN, R.*, et al.*, "Development and biocompatibility of a novel corrodible fluoride-coated magnesium-calcium alloy with improved degradation kinetics and adequate mechanical properties for cardiovascular applications", *Journal of Biomedical Materials Research Part A*, v. 93, n. 2, pp. 763–775, 2010.

[40] CHEN, Q., THOUAS, G.A., "Metallic implant biomaterials", *Materials Science & Engineering R Reports*, v. 87, pp. 1–57, 2015.

[41] IWAOKA, H., HORITA, Z., "Hydrogen behavior in ultrafine-grained palladium processed by high-pressure torsion", *International Journal of Hydrogen Energy*, v. 38, n. 34, pp. 14879–14886, 2013.